Marine Micropaleontology 139 (2018) 28–41

Contents lists available at ScienceDirect

Marine Micropaleontology

journal homepage: www.elsevier.com/locate/marmicro

Research paper

Variability in diatom and silicoflagellate assemblages during mid-Pliocene glacial-interglacial cycles determined in Hole U1361A of IODP Expedition 318, Antarctic Wilkes Land Margin

Linda H. Armbrecht[a,*], Vikki Lowe[a], Carlota Escutia[b], Masao Iwai[c], Robert McKay[d], Leanne K. Armand[a,e]

[a] Department of Biological Sciences/MQMarine, Macquarie University, North Ryde, NSW 2109, Australia
[b] Instituto Andaluz de Ciencias de la Tierra, CSIC - University de Granada, 18100, Armilla (Granada), Spain
[c] Natural Science Cluster/Center for Advanced Marine Core Research, Kochi University, Akebono-cho, Kochi 780-8520, Japan
[d] Antarctic Research Centre, Victoria University of Wellington, Wellington 6140, New Zealand
[e] Research School of Earth Sciences, The Australian National University, Acton ACT 2601, Australia

ARTICLE INFO

Keywords:
Sea-surface temperature
Sea-ice
Fragilariopsis barronii
Rouxia naviculoides
Rouxia antarctica
Denticulopsis simonsenii
Chaetoceros resting spore

ABSTRACT

The Earth is currently experiencing climatic changes that will result in similar environmental conditions to those experienced during the mid-Pliocene (5.3–3.6 million years ago [Ma]), such as similar atmospheric CO_2 concentrations, elevated sea surface temperature, and higher sea-levels due to polar ice melt. Studying the temporal distribution of Antarctic diatoms and silicoflagellates from this epoch provides insights into environmental conditions and sea-ice configurations during that time, and remains the only way to realistically estimate future phytoplankton community responses and Southern Ocean sea-ice extent during large-scale transient changes of similar magnitude to that anticipated by anthropogenic causes. In this study, we identified and quantified diatoms and silicoflagellates in a sediment core section obtained from the Antarctic Wilkes Land margin (IODP Expedition 318, Hole U1361A), spanning four glacial and interglacial cycles around the Gauss/Gilbert geochron boundary (3.6 Ma) between about 3.69 and 3.56 Ma. Two major abundance peaks (around 79.66 and 76.86 mbsf; representing time intervals around 3.65 Ma and 3.58 Ma, respectively) were identified. Both peaks temporally match previously determined high productivity warm intervals (interglacials). Diatom and silicoflagellate assemblages in these two interglacial periods differed: the abundance peak in the older sediments is dominated by the pennate diatoms *Fragilariopsis barronii*, *Rouxia naviculoides* and *Rouxia antarctica*; indicative of seasonal, meltwater associated stratification. The abundance peak in the younger sediments is composed principally of *Chaetoceros* resting spores, suggesting higher productivity, strong stratification and prolonged ice-free, open water conditions. Analysing highly abundant diatoms and environmental indicator species from this IODP Site in relation to the previously determined palaeo-productivity proxy Ba/Al allowed us to refine the age model. Our study provides orbital-scale insights into the variability of Antarctic diatom and silicoflagellate assemblages during the mid-Pliocene, thereby offering a reference for future predictions of extant diatom responses to ongoing climate change.

1. Introduction

Anthropogenic greenhouse gas emissions are currently leading to rapidly increasing global temperatures and climate change. According to latest assessments, atmospheric CO_2 will double and temperatures will increase 1.5°– 4 °C by the end of this century (IPCC, 2013). Under the IPCC RCP8.5 scenario (worst case scenario representing CO_2 concentrations of 936 ppm by 2100) atmospheric CO_2 concentrations will reach the threshold expected to induce continental ice sheet melting (IPCC, 2013; DeConto and Pollard, 2016; Golledge et al., 2016). Melting of Greenland is estimated to contribute ~7.4 m to global sea-level rise (Vasskog et al., 2015) and Antarctic melting is estimated to contribute ~15 m by 2500 (DeConto and Pollard, 2016). While sea-ice in the Arctic has retreated dramatically (~4% decrease in annual mean sea-ice extent per decade, 1979–2012), trends in the Antarctic are less apparent (IPCC, 2013; Jones et al., 2016), however, climatic models simulate a strong Antarctic sea-ice retreat by 2100 (DeConto and Pollard, 2016; Hobbs et al., 2016).

* Corresponding author.
E-mail address: linda.armbrecht@mq.edu.au (L.H. Armbrecht).

https://doi.org/10.1016/j.marmicro.2017.10.008
Received 14 April 2017; Received in revised form 25 October 2017; Accepted 28 October 2017
Available online 18 January 2018
0377-8398/

Studying warmer than present periods, and learning from the physical, chemical and palaeontological data defining such periods, is important to estimate biological and ice sheet responses to the predicted climate conditions (Armand et al., 2017; Golledge et al., 2015, 2017). Today's CO_2 concentrations were last encountered during the warm (early and middle) Pliocene, 5–3.5 Ma, when atmospheric CO_2 was between 330 and 415 ppm (Pagani et al., 2009; Seki et al., 2010). Modelling studies suggest global sea-surface temperatures (SSTs) were between ~1.6–3.6 °C (average ~2.7 °C) warmer than pre-industrial observations (Haywood et al., 2013), with Arctic and Southern Ocean SSTs being about 8 °C and 1–3 °C warmer than today, respectively (Dowsett et al., 2011). Northern hemisphere ice sheets were not fully developed (Zachos et al., 2008) and sea-level changes were driven by fluctuations of the Antarctic ice sheet (Bamber and Aspinall, 2013; Dutton et al., 2015). Sea-level during the Pliocene is estimated to have been 10–30 m higher than today (DeConto and Pollard, 2016).

ANtarctic geological DRILLing (ANDRILL) program and Integrated Ocean Drilling Program (IODP) findings suggest that the marine-based sectors of the West Antarctic Ice Sheet (WAIS) periodically collapsed (Naish et al., 2009; Pollard and DeConto, 2009) and that a substantial retreat of the marine-margin of the East Antarctic Ice Sheet (EAIS) into the Wilkes Land subglacial basins occurred (Cook et al., 2013; Reinardy et al., 2015). The presence of repeated warm periods during the early Pliocene has been demonstrated using silicoflagellate and/or diatom data from around Antarctica (Whitehead and Bohaty, 2003; Grützner et al., 2005; Escutia et al., 2009; Bart and Iwai, 2012; McKay et al., 2012; Winter et al., 2010, 2012a). Based on studies from the Antarctic Wilkes Land margin (Sites U1359 and U1361) successive advances and retreats of the EAIS during the Pliocene have been revealed (Cook et al., 2013; Reinardy et al., 2015).

Marine diatom frustules (siliceous shells, each consisting of two valves) preserved in seafloor sediments are useful proxies for the reconstruction of palaeo-environments and -climate due to the living diatom's high sensitivity to small changes in physical and chemical properties such as temperature, sea-ice cover and salinity (Armand and Leventer, 2010; Armand et al., 2017). Based on Pliocene diatom assemblages in the ANDRILL's McMurdo Ice Shelf project AND-1B drill core from the southwestern Ross Sea, Winter et al. (2010) established a summary of relationships between abundant Southern Ocean/Antarctic sea-ice species and environmental conditions (sea-ice/cold; warm; heavy/wind-mixed; mixed; neritic/stratified). The latter study is the most comprehensive and exhaustive in high southern latitudes to date inferring environmental preferences of extinct species from co-occurrence with modern species, for which preferences are better understood.

In this study, we investigate diatom and silicoflagellate assemblages from IODP Site U1361A (Antarctic Wilkes Land margin) between ~3.69 and 3.56 Ma within the Pliocene, a time period including the Gauss/Gilbert boundary at 3.6 Ma. Being located upstream of the AND-1B site with respect to modern Antarctic Circumpolar Current flow, our results are directly comparable to microfossil assemblages from the latter core discussed in Winter et al. (2010) while providing an intermediate location between the AND-1B site and another site with mid-Pliocene records (Site 1165, Prydz Bay; Whitehead and Bohaty, 2003; Escutia et al., 2009), along a zonal transect of the easterly Antarctic slope current. Previous studies of Pliocene core sections from Site U1361A have shown that EAIS retreats (advances) were associated with high productivity, diatom-rich (low productivity, diatom-poor) sediments (Escutia et al., 2011; Cook et al., 2013; Reinardy et al., 2015). High and low productivity intervals (interglacials and glacials, respectively) were, in addition to diatom counts, determined using the palaeoproductivity proxy Ba/Al (Cook et al., 2013). Our focus is on a well-constrained series of glacial-interglacial (GI) cycles of variable amplitude across the Gauss/Gilbert boundary (Lisiecki and Raymo, 2005) at IODP Site U1361A. These cycles are characterised by a high-amplitude glacial to interglacial cycle (Marine Isotope Stages Gi4-Gi3) that reverts to a high amplitude Gi2 glacial (an ~0.45‰ positive $\delta^{18}O$ excursion), before transitioning into a period when glacial to interglacial variability is muted (e.g., Marine Isotope Stage Gi1 and Mg11), which are separated by a lower amplitude glacial (Mg12; a ~0.25‰ positive $\delta^{18}O$ excursion) coinciding with the Gauss/Gilbert boundary (Lisiecki and Raymo, 2005). We here provide high-resolution insights into the composition of the diatom and silicoflagellate assemblages across these cycles. Our specific objectives are to:

(i) investigate whether peaks in total microfossil abundances coincide with interglacial periods and times of increased productivity as described (using diatom valve concentrations and Ba/Al ratios) in Cook et al. (2013);
(ii) determine the most abundant species across glacial and interglacial periods;
(iii) determine 'environmental indicator species' also found by Winter et al. (2010) in AND-1B, which can be used to establish a constrained age model for the investigated time period.

The question is explored whether phytoplankton communities during such productive interglacial periods were highly similar or differ widely.

2. Methods

2.1. Samples and study site

Cores at the Antarctic Wilkes Land rise Site U1361 (Hole U1361A), East Antarctica, were obtained during IODP Expedition 318 (3 January – 8 March 2010) (Fig. 1). Details specific to the expedition and the investigated core, U1361A-9H (64°24.5728′S, 143°53.1992′E), can be found in Escutia et al. (2011). Subsamples of 2 cm^3 were taken at 20 cm intervals from core sections 1 W–4 W (27 samples, Supplementary Material A) and processed and analysed as detailed in Sections 2.2–2.4.

To provide environmental context to our core data visually, modelled "warm Antarctica" Pliocene conditions over East Antarctica were added to our site map (Fig. 1). Mid-Pliocene orbital forcing was dominated by decreasing variability in obliquity, minimal summer insolation variations at 75°S and low variability around mean annual insolation (Naish et al., 2009; Patterson et al., 2014). Near-surface winds over the Antarctic during the mid-Pliocene have been reported as mainly katabatic. Models suggest that in the Wilkes Land region katabatic winds blew partly over but mostly away from the Transantarctic Mountains towards the open ocean with wind speeds of up to ~12 m s^{-1} (Scherer et al., 2016; Fig. 1).

2.2. Slide preparation

Permanent and cleaned slides for identification and enumeration of diatoms were prepared from all samples following modified methods from Koizumi and Tanimura (1985) (Table 1). Approximately 1 cm^3 of each sediment sample was dried in an oven at 60 °C for 24 h. After cooling to room temperature, 50 mg subsamples were weighed, mixed with 2 mL of 15% H_2O_2 in a 14 mL polypropylene centrifugation tube and placed in a water bath at 60 °C to boil for ~30 min. Subsequently, the tubes were filled up to 10 mL with Milli-Q water, homogenised by gentle shaking, and left to settle overnight. The supernatant was removed by pipetting until the settled material and ~1 mL liquid was left in the tube. This decanting procedure was repeated 5 times, using Milli-Q to resuspend the settled 1 mL residue in runs 1 and 3–5, while in run 2 a solution of 0.01 N sodium diphosphate decahydrate ($Na_4P_2O_7$*$10H_2O$, FW: 446.06) was used for an improved dispersion of clay minerals. After run 5, the tube was filled with Milli-Q to exactly 10 mL and gently mixed. It should be noted that centrifugation was avoided to prevent any breakage of diatoms (Koizumi and Tanimura, 1985).

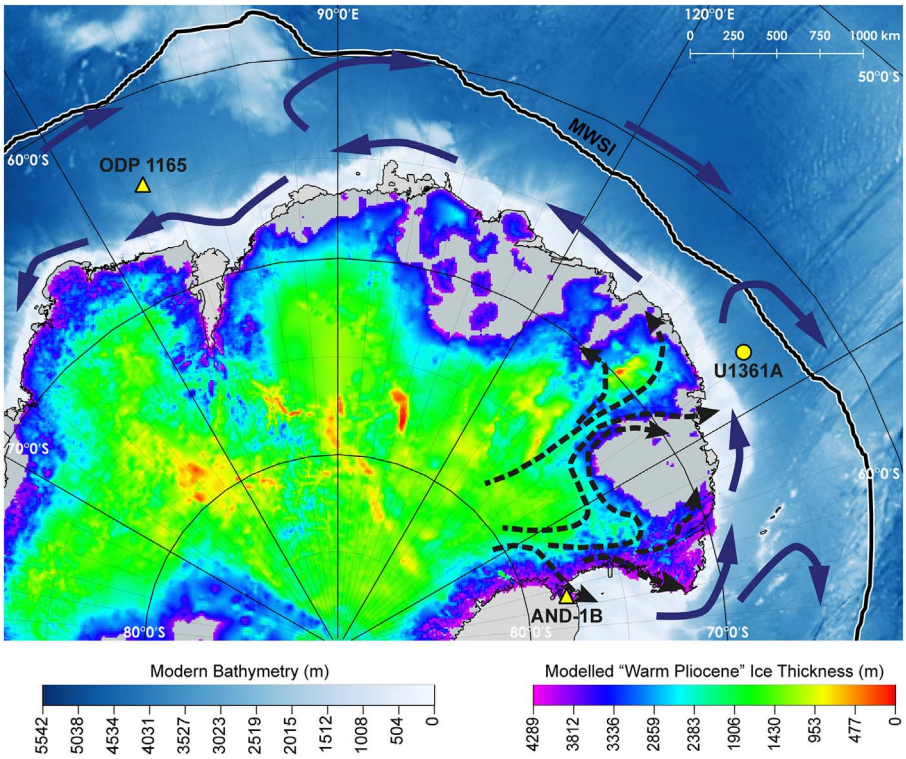

Fig. 1. Site Map. Core site U1361A Expedition 318 (yellow circle) placed in context to modelled "warm Antarctica" ice thickness conditions considered representative of the late Pliocene (Pollard et al., 2015; 10 kyr output) inclusive of modelled mid-Pliocene surface wind conditions relative to U1361A (Scherer et al., 2016; dashed black arrows). Cores AND-1B and ODP1165 are indicated by yellow triangles. Modern land and ice shelf (SCAR, n.d.) and GMRT 3.0 bathymetry (Ryan et al., 2009) are shown with the modern median winter sea-ice extent (MWSI; Fetterer et al., 2016). Modern oceanographic currents (dark blue arrowed lines) after Williams et al. (2010) Fig. 4. Map created by J. L. Lieser (University of Tasmania), with qGIS 2.18, additional lines and annotations by L. Armand using Adobe Illustrator CS6. (For interpretation of the references to colour in this figure legend, the reader is referred to the web version of this article.)

Triplicate subsamples of 25 µL mixed with 975 µL Milli-Q (i.e., a 1 mL solution containing 0.125 mg dry weight) were then strewn evenly onto a potato-starch pre-treated coverslip (22 × 22 mm). The coverslips were dried on a slide warmer (40 °C) for ~2 h. For samples representing 78.86, 79.06, 79.26 and 80.56 m below seafloor (mbsf; see Supplementary Material A) the concentration was increased 3-fold due to low diatom content. The dried coverslips were mounted on a microscope slide using Norland Optical Adhesive 61 and UV light exposure for 10 min.

2.3. Counting

The counting procedure followed Schrader and Gersonde (1978) and Zielinski (1993). However, instead of counting individual field of views, we counted 100 µm wide transects across the coverslip (defined by the outer edges of a scale bar integrated in the objectives) using an Olympus BH-2 compound microscope at a final magnification of 1000 × oil immersion. At least 100 valves were counted along two transects. If the number of counted valves was < 100, an additional two transects were counted as described above. The sample representing 79.26 mbsf, however, contained almost exclusively highly fragmented valves, so that 100 valves could not be reached even after a 5-fold concentration of the sample.

Chaetoceros resting spores were considered to represent two valves to enable direct comparisons to the abundance of valves of other species (acknowledging that this might infer a slight overestimate of diatom abundances). Apices of *Thalassiothrix* and *Thalassionema* were counted as 0.5 valves. Throughout this study the silicoflagellate *Distephanus speculum* is referred to as *Stephanocha speculum* after being recently renamed (Jordan and McCartney, 2015). In the event that we found broken but identifiable diatoms/silicoflagellates, or identifiable species outside our counted transect, these skeletons were photographed and included in our plates despite not being counted (e.g., *Rouxia heteropolara*, *Thalassiosira elliptipora, T. kolbei*, *Actinocyclus* sp./*Dactyliosolen antarcticus*/*Thalassiosira complicata*/*oliverana* girdle bands, *Chaetoceros* setae; Supplementary Material B).

2.4. Analysis

Average species abundances per transect were calculated for each sample. We then applied Eq. (1) to calculate abundance of valves per 1 g dry sediment.

$$\text{Valve abundance} = \text{Av. no. of valves} \times \frac{\text{area coverslip}}{\text{transect coverslip}} \times \frac{1}{\text{dry weight coverslip}} \quad (1)$$

where the area of the coverslip was 4.84 cm^2 and the area of one transect at 1000 × magnification was 0.022 mm^2. Therefore, the scaling factor conversion from 1 transect to 1 coverslip (22 × 22 mm) was 220. The "dry weight coverslip" refers to the volume of sediment under a coverslip, which was in most cases 0.125 mg (see Section 2.2).

Taxa occurring on average > 5% across all samples were considered highly abundant. We identified taxa in our samples recognised by Winter et al. (2010) as environmental indicator species, and assigned the same environmental preferences. Correlation analyses (Pearson) were conducted on the relative abundances of these environmental categories to determine whether different categories co-occurred, providing a more detailed picture of environmental conditions over time.

To test which species might be particularly productive, we conducted Pearson correlation analyses between all taxa and the palaeoproductivity proxy Ba/Al. Specifically, X-ray Fluorescence (XRF)-determined Ba and Al records in Cook et al. (2013) were used to derive a Ba:Al ratio, which was ln transformed prior to graphing and correlation analyses. Ba/Al data was available from the same depths used for diatom and silicoflagellate counts, except for the youngest sediments where the closest Ba/Al data available originated from 4 cm above the count sample.

3. Results

3.1. Abundance and composition

Total diatom and silicoflagellate abundance was estimated to be

Table 1
Diatom and silicoflagellate abundance per sample. Listed are the total abundances for diatoms and silicoflagellates, total for both, and abundances for each species per sample. Units are in valves/g dry sediment for diatoms and skeletons/g dry sediment for silicoflagellates. For the 18 species that could be assigned to environmental categories based on Winter et al. (2010), these categories are indicated after their name.

	Totals			Centric diatoms		
Depth (metres below seafloor, mbsf)	Total fossilised diatoms + silicoflagellates/g dry sediment	Total diatom valves/g dry sediment	Total silicoflagellates/g dry sediment	*Actinocyclus* cf. *dimorphus* (Castracane, 1886) Harwood and Maruyama, 1992	*Actinocyclus ingens* Rattray, 1890	*Actinocyclus karstenii* Van Heurck, 1909 (Cold/Sea-ice)
75.65–75.67	1.48E + 08	1.48E + 08	0.00E + 00	0.00E + 00	0.00E + 00	4.31E + 05
75.85–75.87	1.09E + 08	1.09E + 08	4.40E + 05	0.00E + 00	0.00E + 00	0.00E + 00
76.05–76.07	1.73E + 08	1.70E + 08	2.64E + 06	0.00E + 00	0.00E + 00	0.00E + 00
76.25–76.27	1.67E + 08	1.64E + 08	3.52E + 06	0.00E + 00	0.00E + 00	1.76E + 06
76.45–76.47	2.33E + 08	2.32E + 08	8.80E + 05	0.00E + 00	0.00E + 00	0.00E + 00
76.65–76.67	2.75E + 08	2.70E + 08	4.40E + 06	0.00E + 00	0.00E + 00	8.80E + 05
76.85–76.87	2.75E + 08	2.72E + 08	2.64E + 06	0.00E + 00	0.00E + 00	1.76E + 06
77.35–77.37	1.43E + 08	1.43E + 08	0.00E + 00	0.00E + 00	0.00E + 00	0.00E + 00
77.55–77.57	1.82E + 08	1.80E + 08	2.64E + 06	0.00E + 00	0.00E + 00	4.40E + 06
77.75–77.77	1.26E + 08	1.25E + 08	8.80E + 05	0.00E + 00	8.80E + 05	8.80E + 05
77.95–77.97	1.46E + 08	1.45E + 08	8.63E + 05	0.00E + 00	0.00E + 00	1.73E + 06
78.15–78.17	5.61E + 07	5.61E + 07	0.00E + 00	0.00E + 00	0.00E + 00	1.32E + 06
78.35–78.37	1.15E + 08	1.15E + 08	0.00E + 00	0.00E + 00	0.00E + 00	1.76E + 06
78.65–78.67	4.55E + 07	4.55E + 07	0.00E + 00	0.00E + 00	4.40E + 05	8.80E + 05
78.85–78.87	1.05E + 07	1.05E + 07	0.00E + 00	0.00E + 00	0.00E + 00	9.78E + 04
79.05–79.07	9.63E + 06	9.63E + 06	0.00E + 00	0.00E + 00	9.78E + 04	0.00E + 00
79.25–79.27	4.80E + 06	4.80E + 06	0.00E + 00	0.00E + 00	0.00E + 00	8.80E + 04
79.45–79.47	2.27E + 08	2.22E + 08	5.28E + 06	0.00E + 00	0.00E + 00	3.52E + 06
79.65–79.67	2.82E + 08	2.75E + 08	7.04E + 06	1.76E + 06	0.00E + 00	3.52E + 06
79.85–79.87	2.41E + 08	2.39E + 08	1.76E + 06	0.00E + 00	0.00E + 00	2.64E + 06
80.15–80.17	3.34E + 07	3.31E + 07	2.93E + 05	0.00E + 00	0.00E + 00	5.87E + 05
80.35–80.37	2.66E + 07	2.66E + 07	0.00E + 00	0.00E + 00	0.00E + 00	0.00E + 00
80.55–80.57	1.36E + 07	1.36E + 07	0.00E + 00	0.00E + 00	0.00E + 00	0.00E + 00
80.75–80.77	3.04E + 07	3.04E + 07	0.00E + 00	0.00E + 00	0.00E + 00	0.00E + 00
80.95–80.97	3.43E + 07	3.43E + 07	0.00E + 00	0.00E + 00	8.80E + 05	0.00E + 00
81.15–81.17	4.38E + 07	4.33E + 07	4.40E + 05	0.00E + 00	0.00E + 00	4.40E + 05
81.35–81.37	1.94E + 07	1.94E + 07	0.00E + 00	0.00E + 00	0.00E + 00	0.00E + 00

Azpeitia cf. *tabularis* (Grunow, 1884) Fryxell and Sims in Fryxell et al., 1986	*Azpeitia* spp.	*Chaetoceros* cf. *lorenzianus* Grunow, 1863	*Chaetoceros* sp. 2	*Chaetoceros* sp. 3	*Chaetoceros* sp. 4	*Chaetoceros* resting spore type 1 (Neritic/Stratified)
0.00E + 00	0.00E + 00	2.16E + 06	4.31E + 05	4.31E + 05	0.00E + 00	5.18E + 07
0.00E + 00	0.00E + 00	1.10E + 07	4.40E + 05	4.40E + 05	0.00E + 00	2.29E + 07
0.00E + 00	0.00E + 00	1.32E + 07	1.76E + 06	8.80E + 05	0.00E + 00	5.28E + 07
0.00E + 00	0.00E + 00	1.58E + 07	8.80E + 05	8.80E + 05	8.80E + 05	3.70E + 07
0.00E + 00	0.00E + 00	2.64E + 07	0.00E + 00	1.76E + 06	0.00E + 00	7.22E + 07
0.00E + 00	0.00E + 00	2.38E + 07	0.00E + 00	8.80E + 05	0.00E + 00	8.10E + 07
0.00E + 00	0.00E + 00	1.14E + 07	0.00E + 00	8.80E + 05	0.00E + 00	8.45E + 07
0.00E + 00	0.00E + 00	2.38E + 07	8.80E + 05	0.00E + 00	0.00E + 00	2.64E + 07
0.00E + 00	0.00E + 00	1.06E + 07	0.00E + 00	0.00E + 00	8.80E + 05	2.46E + 07
0.00E + 00	0.00E + 00	2.02E + 07	0.00E + 00	0.00E + 00	0.00E + 00	3.70E + 07
0.00E + 00	0.00E + 00	1.12E + 07	0.00E + 00	0.00E + 00	0.00E + 00	2.93E + 07

(continued on next page)

Table 1 *(continued)*

Azpeitia cf. *tabularis* (Grunow, 1884) Fryxell and Sims in Fryxell et al., 1986	*Azpeitia* spp.	*Chaetoceros* cf. *lorenzianus* Grunow, 1863	*Chaetoceros* sp. 2	*Chaetoceros* sp. 3	*Chaetoceros* sp. 4	*Chaetoceros* resting spore type 1 (Neritic/Stratified)
0.00E + 00	0.00E + 00	5.72E + 06	0.00E + 00	0.00E + 00	0.00E + 00	2.55E + 07
0.00E + 00	0.00E + 00	1.32E + 07	0.00E + 00	0.00E + 00	0.00E + 00	3.52E + 07
0.00E + 00	4.40E + 05	2.64E + 06	0.00E + 00	8.80E + 05	4.40E + 05	1.50E + 07
0.00E + 00	0.00E + 00	2.93E + 05	0.00E + 00	0.00E + 00	0.00E + 00	2.93E + 06
0.00E + 00	0.00E + 00	4.40E + 05	0.00E + 00	0.00E + 00	0.00E + 00	2.93E + 06
0.00E + 00	0.00E + 00	8.80E + 04	0.00E + 00	0.00E + 00	0.00E + 00	8.80E + 05
0.00E + 00	0.00E + 00	6.16E + 06	0.00E + 00	1.76E + 06	0.00E + 00	2.99E + 07
1.76E + 06	0.00E + 00	1.76E + 06	0.00E + 00	0.00E + 00	1.76E + 06	3.87E + 07
0.00E + 00	0.00E + 00	6.16E + 06	1.76E + 06	8.80E + 05	0.00E + 00	2.99E + 07
0.00E + 00	0.00E + 00	2.93E + 06	0.00E + 00	0.00E + 00	0.00E + 00	5.87E + 06
0.00E + 00	0.00E + 00	3.08E + 06	0.00E + 00	0.00E + 00	0.00E + 00	5.28E + 06
0.00E + 00	0.00E + 00	7.33E + 05	0.00E + 00	0.00E + 00	0.00E + 00	3.23E + 06
0.00E + 00	0.00E + 00	8.80E + 05	0.00E + 00	0.00E + 00	0.00E + 00	9.39E + 06
0.00E + 00	0.00E + 00	3.08E + 06	0.00E + 00	0.00E + 00	0.00E + 00	7.04E + 06
0.00E + 00	0.00E + 00	2.20E + 06	0.00E + 00	8.80E + 05	0.00E + 00	7.92E + 06
0.00E + 00	0.00E + 00	8.80E + 05	0.00E + 00	4.40E + 05	0.00E + 00	6.16E + 06

	Centric diatoms						
Depth (metres below seafloor, mbsf)	*Chaetoceros* resting spore type 2 (Neritic/Stratified)	*Chaetoceros* resting spore type 9 (Neritic/Stratified)	Centric sp. 8	Centric sp. 17	*Corethron criophilum* Castracane, 1886	*Eucampia antarctica* (Castracane, 1886) Mangin, 1914 (Heavy/Wind-mixed)	*Hemidiscus karstenii* Jousé, 1965
75.65–75.67	2.85E + 07	0.00E + 00	0.00E + 00	0.00E + 00	0.00E + 00	4.31E + 05	0.00E + 00
75.85–75.87	3.52E + 06	0.00E + 00	0.00E + 00	0.00E + 00	4.40E + 05	0.00E + 00	0.00E + 00
76.05–76.07	1.76E + 06	0.00E + 00	0.00E + 00	0.00E + 00	0.00E + 00	0.00E + 00	0.00E + 00
76.25–76.27	0.00E + 00	0.00E + 00	0.00E + 00	0.00E + 00	0.00E + 00	8.80E + 05	0.00E + 00
76.45–76.47	3.52E + 06	0.00E + 00	0.00E + 00	0.00E + 00	0.00E + 00	4.40E + 06	0.00E + 00
76.65–76.67	5.28E + 06	0.00E + 00	8.80E + 05	0.00E + 00	0.00E + 00	8.80E + 05	0.00E + 00
76.85–76.87	1.94E + 07	5.28E + 06	8.80E + 05	0.00E + 00	0.00E + 00	0.00E + 00	0.00E + 00
77.35–77.37	0.00E + 00	0.00E + 00	0.00E + 00	0.00E + 00	0.00E + 00	8.80E + 05	0.00E + 00
77.55–77.57	1.76E + 06	0.00E + 00	0.00E + 00	0.00E + 00	0.00E + 00	0.00E + 00	0.00E + 00
77.75–77.77	0.00E + 00	0.00E + 00	0.00E + 00	0.00E + 00	0.00E + 00	8.80E + 05	0.00E + 00
77.95–77.97	8.63E + 06	0.00E + 00	0.00E + 00	0.00E + 00	0.00E + 00	8.63E + 05	8.63E + 05
78.15–78.17	4.40E + 06	0.00E + 00	0.00E + 00	0.00E + 00	0.00E + 00	0.00E + 00	0.00E + 00
78.35–78.37	7.04E + 06	0.00E + 00	0.00E + 00	0.00E + 00	0.00E + 00	8.80E + 05	0.00E + 00
78.65–78.67	2.64E + 06	0.00E + 00	0.00E + 00	0.00E + 00	0.00E + 00	0.00E + 00	0.00E + 00
78.85–78.87	1.96E + 05	0.00E + 00	0.00E + 00	0.00E + 00	0.00E + 00	0.00E + 00	0.00E + 00
79.05–79.07	2.93E + 05	0.00E + 00	0.00E + 00	0.00E + 00	0.00E + 00	0.00E + 00	0.00E + 00
79.25–79.27	3.52E + 05	0.00E + 00	0.00E + 00	0.00E + 00	0.00E + 00	0.00E + 00	0.00E + 00
79.45–79.47	3.52E + 06	0.00E + 00	0.00E + 00	0.00E + 00	0.00E + 00	1.76E + 06	0.00E + 00
79.65–79.67	7.04E + 06	0.00E + 00	0.00E + 00	0.00E + 00	0.00E + 00	1.76E + 06	0.00E + 00
79.85–79.87	1.58E + 07	0.00E + 00	0.00E + 00	0.00E + 00	0.00E + 00	0.00E + 00	0.00E + 00
80.15–80.17	5.87E + 05	0.00E + 00	0.00E + 00	2.93E + 05	0.00E + 00	2.93E + 05	0.00E + 00
80.35–80.37	8.80E + 05	0.00E + 00	0.00E + 00	0.00E + 00	0.00E + 00	0.00E + 00	0.00E + 00
80.55–80.57	8.80E + 05	0.00E + 00	0.00E + 00	0.00E + 00	0.00E + 00	0.00E + 00	0.00E + 00
80.75–80.77	1.76E + 06	0.00E + 00	0.00E + 00	0.00E + 00	0.00E + 00	5.87E + 05	0.00E + 00
80.95–80.97	8.80E + 05	0.00E + 00	0.00E + 00	0.00E + 00	0.00E + 00	0.00E + 00	0.00E + 00

(continued on next page)

Table 1 *(continued)*

Depth (metres below seafloor, mbsf)	Centric diatoms						
	Chaetoceros resting spore type 2 (Neritic/Stratified)	*Chaetoceros* resting spore type 9 (Neritic/Stratified)	Centric sp. 8	Centric sp. 17	*Corethron criophilum* Castracane, 1886	*Eucampia antarctica* (Castracane, 1886) Mangin, 1914 (Heavy/Wind-mixed)	*Hemidiscus karstenii* Jousé, 1965
81.15–81.17	1.76E + 06	0.00E + 00	0.00E + 00	0.00E + 00	0.00E + 00	0.00E + 00	0.00E + 00
81.35–81.37	1.76E + 06	0.00E + 00	0.00E + 00	0.00E + 00	0.00E + 00	0.00E + 00	0.00E + 00

Rhizosolenia sp. 1	*Rhizosolenia* sp. 2	*Shionodiscus oestrupii* (Ostenfield, 1900) Alverson et al., 2006 (Warm)	*Stephanopyxis turris* (Greville and Arnott) Ralfs in Pritchard, 1861 (Heavy/Wind-mixed)	*Thalassiosira complicata* Gersonde, 1991 (Mixed)	*Thalassiosira inura* Gersonde, 1991 (Mixed)	*Thalassiosira oliverana* (O'Meara, 1876) Makarova and Nikolaev, 1983
4.31E + 05	4.31E + 05	4.31E + 06	4.31E + 05	0.00E + 00	5.61E + 06	0.00E + 00
4.40E + 05	1.32E + 06	9.68E + 06	0.00E + 00	1.76E + 06	7.04E + 06	0.00E + 00
0.00E + 00	1.76E + 06	1.23E + 07	1.76E + 06	1.76E + 06	5.28E + 06	0.00E + 00
1.76E + 06	1.76E + 06	1.23E + 07	1.76E + 06	8.80E + 05	1.23E + 07	0.00E + 00
0.00E + 00	3.52E + 06	1.41E + 07	0.00E + 00	8.80E + 05	1.06E + 07	0.00E + 00
0.00E + 00	8.80E + 05	1.76E + 07	0.00E + 00	1.76E + 06	1.32E + 07	0.00E + 00
0.00E + 00	1.76E + 06	1.41E + 07	0.00E + 00	8.80E + 05	1.41E + 07	0.00E + 00
2.64E + 06	3.52E + 06	2.64E + 06	0.00E + 00	0.00E + 00	1.41E + 07	0.00E + 00
0.00E + 00	1.76E + 06	3.52E + 06	8.80E + 05	1.76E + 06	1.76E + 07	0.00E + 00
0.00E + 00	2.64E + 06	0.00E + 00	8.80E + 05	0.00E + 00	9.68E + 06	0.00E + 00
8.63E + 05	0.00E + 00	5.18E + 06	0.00E + 00	6.90E + 06	2.59E + 06	8.63E + 05
0.00E + 00	0.00E + 00	1.76E + 06	4.40E + 05	0.00E + 00	1.76E + 06	0.00E + 00
8.80E + 05	8.80E + 05	1.76E + 06	8.80E + 05	8.80E + 05	6.16E + 06	0.00E + 00
0.00E + 00	2.64E + 06	4.40E + 05	4.40E + 05	0.00E + 00	3.08E + 06	0.00E + 00
9.78E + 04	9.78E + 04	1.96E + 05	0.00E + 00	0.00E + 00	8.80E + 05	0.00E + 00
2.93E + 05	4.40E + 05	4.40E + 05	0.00E + 00	0.00E + 00	2.93E + 05	0.00E + 00
5.28E + 05	8.80E + 04	0.00E + 00	0.00E + 00	0.00E + 00	0.00E + 00	0.00E + 00
8.80E + 05	8.80E + 05	1.76E + 06	2.64E + 06	8.80E + 05	2.02E + 07	0.00E + 00
0.00E + 00	0.00E + 00	0.00E + 00	3.52E + 06	1.76E + 06	1.06E + 07	0.00E + 00
0.00E + 00	1.76E + 06	3.52E + 06	0.00E + 00	1.76E + 06	2.02E + 07	0.00E + 00
0.00E + 00	1.76E + 06	8.80E + 05	2.93E + 05	0.00E + 00	1.47E + 06	0.00E + 00
1.32E + 06	1.32E + 06	0.00E + 00	0.00E + 00	0.00E + 00	4.40E + 05	0.00E + 00
5.87E + 05	0.00E + 00	2.93E + 05	0.00E + 00	0.00E + 00	0.00E + 00	0.00E + 00
5.87E + 05	2.93E + 05	8.80E + 05	0.00E + 00	2.93E + 05	1.17E + 06	0.00E + 00
8.80E + 05	4.40E + 05	3.08E + 06	4.40E + 05	0.00E + 00	0.00E + 00	0.00E + 00
8.80E + 05	0.00E + 00	0.00E + 00	0.00E + 00	4.40E + 05	7.48E + 06	0.00E + 00
0.00E + 00	4.40E + 05	8.80E + 05	0.00E + 00	0.00E + 00	4.40E + 05	0.00E + 00

Depth (metres below seafloor, mbsf)	Centric Diatoms						
	Thalassiosira striata Harwood & Maruyama, 1992 (Cold/Sea-ice)	*Thalassiosira* sp. 1	*Thalassiosira* sp. 3	*Thalassiosira* sp. 5	*Thalassiosira* sp. 6	*Thalassiosira* sp. 9	*Thalassiosira* sp. 10
75.65–75.67	1.73E + 06	4.31E + 05	8.63E + 05	4.31E + 05	3.45E + 06	0.00E + 00	0.00E + 00
75.85–75.87	4.40E + 05	0.00E + 00	8.80E + 05	0.00E + 00	2.20E + 06	4.40E + 05	0.00E + 00
76.05–76.07	8.80E + 05	0.00E + 00	0.00E + 00	0.00E + 00	1.76E + 06	0.00E + 00	0.00E + 00
76.25–76.27	2.64E + 06	0.00E + 00	0.00E + 00	0.00E + 00	2.64E + 06	8.80E + 05	0.00E + 00
76.45–76.47	8.80E + 05	0.00E + 00	1.76E + 06	0.00E + 00	8.80E + 05	0.00E + 00	0.00E + 00
76.65–76.67	2.64E + 06	0.00E + 00	0.00E + 00	0.00E + 00	8.80E + 05	0.00E + 00	0.00E + 00
76.85–76.87	8.80E + 05	0.00E + 00	0.00E + 00	0.00E + 00	8.80E + 05	0.00E + 00	0.00E + 00
77.35–77.37	0.00E + 00	0.00E + 00	0.00E + 00	0.00E + 00	8.80E + 05	0.00E + 00	0.00E + 00
77.55–77.57	0.00E + 00	0.00E + 00	0.00E + 00	8.80E + 05	1.76E + 06	0.00E + 00	0.00E + 00

(continued on next page)

Table 1 *(continued)*

	Centric Diatoms						
Depth (metres below seafloor, mbsf)	*Thalassiosira striata* Harwood & Maruyama, 1992 (Cold/Sea-ice)	*Thalassiosira* sp. 1	*Thalassiosira* sp. 3	*Thalassiosira* sp. 5	*Thalassiosira* sp. 6	*Thalassiosira* sp. 9	*Thalassiosira* sp. 10
77.75–77.77	0.00E + 00	0.00E + 00	0.00E + 00	2.64E + 06	0.00E + 00	0.00E + 00	0.00E + 00
77.95–77.97	1.73E + 06	0.00E + 00	0.00E + 00	0.00E + 00	8.63E + 05	0.00E + 00	0.00E + 00
78.15–78.17	8.80E + 05	0.00E + 00	0.00E + 00	4.40E + 05	8.80E + 05	0.00E + 00	0.00E + 00
78.35–78.37	0.00E + 00	0.00E + 00	0.00E + 00	0.00E + 00	8.80E + 05	0.00E + 00	0.00E + 00
78.65–78.67	4.40E + 05	0.00E + 00	4.40E + 05	0.00E + 00	0.00E + 00	0.00E + 00	0.00E + 00
78.85–78.87	1.96E + 05	0.00E + 00	0.00E + 00	0.00E + 00	9.78E + 04	0.00E + 00	0.00E + 00
79.05–79.07	1.47E + 05	0.00E + 00	0.00E + 00	0.00E + 00	0.00E + 00	0.00E + 00	0.00E + 00
79.25–79.27	0.00E + 00	0.00E + 00	0.00E + 00	0.00E + 00	0.00E + 00	0.00E + 00	0.00E + 00
79.45–79.47	0.00E + 00	0.00E + 00	0.00E + 00	0.00E + 00	1.76E + 06	0.00E + 00	0.00E + 00
79.65–79.67	0.00E + 00	0.00E + 00	0.00E + 00	0.00E + 00	3.52E + 06	0.00E + 00	1.76E + 06
79.85–79.87	0.00E + 00	0.00E + 00	0.00E + 00	0.00E + 00	1.76E + 06	3.52E + 06	0.00E + 00
80.15–80.17	2.93E + 05	0.00E + 00	2.93E + 05	0.00E + 00	0.00E + 00	0.00E + 00	0.00E + 00
80.35–80.37	0.00E + 00	0.00E + 00	0.00E + 00	0.00E + 00	4.40E + 05	0.00E + 00	0.00E + 00
80.55–80.57	0.00E + 00	0.00E + 00	1.47E + 05	0.00E + 00	0.00E + 00	0.00E + 00	0.00E + 00
80.75–80.77	0.00E + 00	0.00E + 00	0.00E + 00	0.00E + 00	2.93E + 05	2.93E + 05	0.00E + 00
80.95–80.97	0.00E + 00	0.00E + 00	1.32E + 06	0.00E + 00	4.40E + 05	1.32E + 06	0.00E + 00
81.15–81.17	0.00E + 00	0.00E + 00	0.00E + 00	0.00E + 00	0.00E + 00	0.00E + 00	0.00E + 00
81.35–81.37	0.00E + 00	0.00E + 00	0.00E + 00	0.00E + 00	0.00E + 00	0.00E + 00	0.00E + 00

	Pennate diatoms					
Trinacria excavata Heiberg, 1863	*Cocconeis costata* Gregory, 1855	*Denticulopsis simonsenii* Yanagisawa and Akiba, 1990	*Fragilariopsis barronii* (Gersonde. 1991) Gersonde and Bárcena, 1998	*Fragilariopsis curta* (Van Heurck, 1909) Hustedt, 1958 (Cold/Sea-ice)	*Frgilariopsis praecurta* (Gersonde, 1991) Gersonde and Bárcena, 1998	*Fragilariopsis praeinterfragidaria* (McCollum, 1975) Gersonde and Bárcena, 1998 (Mixed)
0.00E + 00	0.00E + 00	8.63E + 05	3.45E + 06	1.29E + 06	3.02E + 06	6.04E + 06
0.00E + 00	0.00E + 00	4.40E + 05	3.52E + 06	1.76E + 06	0.00E + 00	3.96E + 06
0.00E + 00	0.00E + 00	0.00E + 00	2.64E + 06	1.76E + 06	0.00E + 00	5.28E + 06
0.00E + 00	0.00E + 00	8.80E + 05	5.28E + 06	8.80E + 05	8.80E + 05	9.68E + 06
0.00E + 00	0.00E + 00	8.80E + 05	2.64E + 06	6.16E + 06	0.00E + 00	1.06E + 07
0.00E + 00	0.00E + 00	1.76E + 06	1.50E + 07	8.80E + 05	0.00E + 00	7.92E + 06
0.00E + 00	8.80E + 05	0.00E + 00	1.76E + 07	2.64E + 06	2.64E + 06	6.16E + 06
0.00E + 00	0.00E + 00	0.00E + 00	8.80E + 06	0.00E + 00	0.00E + 00	1.76E + 06
0.00E + 00	0.00E + 00	8.80E + 05	2.11E + 07	0.00E + 00	0.00E + 00	7.04E + 06
0.00E + 00	0.00E + 00	8.80E + 05	8.80E + 06	3.52E + 06	0.00E + 00	3.52E + 06
0.00E + 00	0.00E + 00	8.63E + 05	1.21E + 07	1.73E + 06	5.18E + 06	6.90E + 06
0.00E + 00	0.00E + 00	0.00E + 00	8.80E + 05	4.40E + 05	0.00E + 00	1.76E + 06
0.00E + 00	0.00E + 00	1.76E + 06	5.28E + 06	8.80E + 05	0.00E + 00	2.64E + 06
0.00E + 00	4.40E + 05	4.40E + 05	2.64E + 06	8.80E + 05	0.00E + 00	2.20E + 06
0.00E + 00	0.00E + 00	3.91E + 05	3.91E + 05	1.96E + 05	0.00E + 00	6.84E + 05
0.00E + 00	1.47E + 05	1.32E + 06	1.47E + 05	2.93E + 05	0.00E + 00	4.40E + 05
0.00E + 00	8.80E + 04	7.04E + 05	8.80E + 04	8.80E + 04	0.00E + 00	0.00E + 00
0.00E + 00	0.00E + 00	0.00E + 00	2.64E + 07	1.76E + 06	0.00E + 00	1.06E + 07
0.00E + 00	0.00E + 00	0.00E + 00	5.46E + 07	8.80E + 06	0.00E + 00	1.06E + 07
0.00E + 00	0.00E + 00	8.80E + 05	5.72E + 07	1.76E + 06	0.00E + 00	1.76E + 07
0.00E + 00	0.00E + 00	5.87E + 06	5.87E + 05	5.87E + 05	0.00E + 00	8.80E + 05
0.00E + 00	0.00E + 00	8.36E + 06	0.00E + 00	0.00E + 00	1.32E + 06	4.40E + 05
1.47E + 05	0.00E + 00	2.35E + 06	2.93E + 05	4.40E + 05	1.47E + 05	1.17E + 06
0.00E + 00	0.00E + 00	2.64E + 06	2.35E + 06	0.00E + 00	0.00E + 00	1.17E + 06

(continued on next page)

Table 1 *(continued)*

	Pennate diatoms					
Trinacria excavata Heiberg, 1863	*Cocconeis costata* Gregory, 1855	*Denticulopsis simonsenii* Yanagisawa and Akiba, 1990	*Fragilariopsis barronii* (Gersonde. 1991) Gersonde and Bárcena, 1998	*Fragilariopsis curta* (Van Heurck, 1909) Hustedt, 1958 (Cold/Sea-ice)	*Frgilariopsis praecurta* (Gersonde, 1991) Gersonde and Bárcena, 1998	*Fragilariopsis praeinterfragidaria* (McCollum, 1975) Gersonde and Bárcena, 1998 (Mixed)
0.00E + 00	0.00E + 00	1.76E + 06	8.80E + 05	8.80E + 05	0.00E + 00	1.76E + 06
0.00E + 00	0.00E + 00	5.72E + 06	2.64E + 06	0.00E + 00	8.80E + 05	3.08E + 06
0.00E + 00	0.00E + 00	8.80E + 05	1.76E + 06	8.80E + 05	0.00E + 00	4.40E + 05

	Pennate diatoms						
Depth (metres below seafloor, mbsf)	*Fragilariopsis weaveri* (Ciesielski, 1983) Gersonde and Bárcena, 1998	Pennate sp. 3	Pennate sp. 11	*Rouxia antarctica* Heiden in Heiden and Kolbe, 1928 (Cold/Sea-ice)	*Rouxia diploneides* Schrader, 1973a (Cold/Sea-ice)	*Rouxia* cf. *isopolica* Schrader, 1976 (Cold/Sea-ice)	*Rouxia naviculoides* Schrader, 1973a (Cold/Sea-ice)
75.65–75.67	0.00E + 00	4.31E + 05	2.59E + 06	9.49E + 06	3.02E + 06	2.59E + 06	8.20E + 06
75.85–75.87	6.16E + 06	0.00E + 00	1.32E + 06	7.48E + 06	5.28E + 06	2.20E + 06	1.01E + 07
76.05–76.07	5.28E + 06	8.80E + 05	5.28E + 06	1.94E + 07	1.06E + 07	4.40E + 06	1.41E + 07
76.25–76.27	4.40E + 06	0.00E + 00	1.76E + 06	9.68E + 06	7.92E + 06	2.64E + 06	1.85E + 07
76.45–76.47	9.68E + 06	0.00E + 00	2.64E + 06	1.32E + 07	7.92E + 06	5.28E + 06	2.46E + 07
76.65–76.67	1.14E + 07	0.00E + 00	2.64E + 06	1.94E + 07	5.28E + 06	4.40E + 06	4.05E + 07
76.85–76.87	1.67E + 07	0.00E + 00	4.40E + 06	1.58E + 07	6.16E + 06	6.16E + 06	2.99E + 07
77.35–77.37	1.41E + 07	0.00E + 00	1.76E + 06	7.92E + 06	0.00E + 00	8.80E + 05	2.20E + 07
77.55–77.57	8.80E + 06	0.00E + 00	8.80E + 05	2.29E + 07	8.80E + 06	1.06E + 07	2.20E + 07
77.75–77.77	4.40E + 06	0.00E + 00	0.00E + 00	8.80E + 06	0.00E + 00	2.64E + 06	1.14E + 07
77.95–77.97	4.31E + 06	0.00E + 00	3.45E + 06	8.63E + 06	6.90E + 06	8.63E + 06	1.21E + 07
78.15–78.17	4.40E + 05	0.00E + 00	8.80E + 05	1.32E + 06	4.40E + 05	8.80E + 05	4.40E + 06
78.35–78.37	1.76E + 06	0.00E + 00	0.00E + 00	9.68E + 06	1.76E + 06	9.68E + 06	9.68E + 06
78.65–78.67	0.00E + 00	0.00E + 00	1.32E + 06	3.08E + 06	0.00E + 00	1.32E + 06	1.76E + 06
78.85–78.87	2.93E + 05	0.00E + 00	2.93E + 05	8.80E + 05	1.96E + 05	1.08E + 06	5.87E + 05
79.05–79.07	0.00E + 00	0.00E + 00	1.47E + 05	2.93E + 05	2.93E + 05	2.93E + 05	1.47E + 05
79.25–79.27	0.00E + 00	0.00E + 00	2.64E + 05	1.76E + 05	8.80E + 04	4.40E + 05	2.64E + 05
79.45–79.47	7.04E + 06	0.00E + 00	1.94E + 07	1.67E + 07	5.28E + 06	2.82E + 07	2.38E + 07
79.65–79.67	1.76E + 06	0.00E + 00	0.00E + 00	4.22E + 07	7.04E + 06	2.29E + 07	4.22E + 07
79.85–79.87	7.04E + 06	0.00E + 00	1.76E + 06	2.46E + 07	4.40E + 06	7.92E + 06	2.46E + 07
80.15–80.17	2.93E + 05	0.00E + 00	2.93E + 05	2.93E + 06	1.76E + 06	8.80E + 05	2.05E + 06
80.35–80.37	0.00E + 00	4.40E + 05	4.40E + 05	4.40E + 05	4.40E + 05	0.00E + 00	4.40E + 05
80.55–80.57	0.00E + 00	0.00E + 00	5.87E + 05	4.40E + 05	1.47E + 05	4.40E + 05	5.87E + 05
80.75–80.77	0.00E + 00	2.93E + 05	2.93E + 05	2.64E + 06	5.87E + 05	1.17E + 06	2.05E + 06
80.95–80.97	0.00E + 00	0.00E + 00	3.08E + 06	1.76E + 06	8.80E + 05	1.32E + 06	4.40E + 05
81.15–81.17	0.00E + 00	0.00E + 00	4.40E + 05	1.32E + 06	4.40E + 05	3.52E + 06	2.20E + 06
81.35–81.37	0.00E + 00	0.00E + 00	4.40E + 05	4.40E + 05	1.32E + 06	4.40E + 05	1.32E + 06

(continued on next page)

Table 1 *(continued)*

cf. *Synedra* spp.	cf. *Synedropsis* spp.	*Thalassionema nitzschioides* (Grunow in Van Heurck) Mereschkowsky (Neritic/Stratified)	*Thalassiothrix antarctica* Schimper ex Karsten 1905	*Thalassiothrix longissima* Cleve and Grunow, 1880	Silico-flagellates
					Stephanocha speculum (previously *Dictyocha speculum* Ehrenberg, 1839, see Jordan and McCartney, 2015) (Heavy/Wind-mixed)
0.00E + 00	1.29E + 06	2.16E + 06	2.16E + 05	6.47E + 05	0.00E + 00
0.00E + 00	4.40E + 05	1.10E + 06	6.60E + 05	1.32E + 06	4.40E + 05
0.00E + 00	8.80E + 05	8.80E + 05	1.76E + 06	1.32E + 06	2.64E + 06
0.00E + 00	0.00E + 00	2.64E + 06	8.80E + 05	2.64E + 06	3.52E + 06
0.00E + 00	8.80E + 05	5.28E + 06	8.80E + 05	4.40E + 05	8.80E + 05
0.00E + 00	3.52E + 06	4.40E + 06	8.80E + 05	1.76E + 06	4.40E + 06
8.80E + 05	0.00E + 00	4.40E + 06	4.40E + 05	4.40E + 05	2.64E + 06
0.00E + 00	0.00E + 00	1.76E + 06	3.52E + 06	5.28E + 06	0.00E + 00
0.00E + 00	2.64E + 06	1.76E + 06	8.80E + 05	8.80E + 05	2.64E + 06
0.00E + 00	0.00E + 00	3.52E + 06	1.32E + 06	8.80E + 05	8.80E + 05
8.63E + 05	0.00E + 00	1.73E + 06	0.00E + 00	0.00E + 00	8.63E + 05
0.00E + 00	0.00E + 00	1.32E + 06	2.20E + 05	0.00E + 00	0.00E + 00
0.00E + 00	0.00E + 00	1.76E + 06	0.00E + 00	0.00E + 00	0.00E + 00
0.00E + 00	0.00E + 00	2.20E + 05	2.20E + 05	2.20E + 05	0.00E + 00
0.00E + 00	0.00E + 00	2.93E + 05	1.47E + 05	0.00E + 00	0.00E + 00
0.00E + 00	0.00E + 00	7.33E + 05	0.00E + 00	0.00E + 00	0.00E + 00
0.00E + 00	1.76E + 05	3.52E + 05	4.40E + 04	0.00E + 00	0.00E + 00
0.00E + 00	5.28E + 06	8.80E + 05	0.00E + 00	8.80E + 05	5.28E + 06
0.00E + 00	1.76E + 06	1.76E + 06	8.80E + 05	8.80E + 05	7.04E + 06
0.00E + 00	0.00E + 00	0.00E + 00	4.40E + 05	8.80E + 05	1.76E + 06
0.00E + 00	0.00E + 00	1.03E + 06	1.47E + 05	2.93E + 05	2.93E + 05
0.00E + 00	0.00E + 00	1.32E + 06	0.00E + 00	2.20E + 05	0.00E + 00
0.00E + 00	1.47E + 05	8.80E + 05	0.00E + 00	0.00E + 00	0.00E + 00
0.00E + 00	2.93E + 05	4.40E + 05	0.00E + 00	0.00E + 00	0.00E + 00
0.00E + 00	0.00E + 00	1.32E + 06	2.20E + 05	2.20E + 05	0.00E + 00
0.00E + 00	0.00E + 00	8.80E + 05	0.00E + 00	2.20E + 05	4.40E + 05
0.00E + 00	4.40E + 05	0.00E + 00	0.00E + 00	0.00E + 00	0.00E + 00

between 4.80×10^6 and 2.82×10^8 microfossils/per g dry sediment (valves/g dry sediment and skeletons/g dry sediment for diatoms and silicoflagellates, respectively) (Fig. 2C). Diatoms comprised the bulk of the assemblages (reaching from 4.8×10^6 to 2.75×10^8 valves/g dry sediment, Fig. 2C) while silicoflagellates were observed in much lower abundances (0 to 7.06×10^6 skeletons/g dry sediment, Fig. 2C). Two periods of increased abundance are identified in the core: one abundance peak (2.82×10^8 diatoms + silicoflagellates/g dry sediment) occurred at 79.66 mbsf, after which abundances decreased to 4.8×10^6 diatoms + silicoflagellates/g dry sediment at 79.26 mbsf. Around 76.86 mbsf another abundance peak was observed (2.75×10^8 diatoms + silicoflagellates/g dry sediment), after which abundances decreased gradually to approximately half the peak-maximum (1.09×10^8 diatoms + silicoflagellates/g dry sediment) in our second uppermost/youngest sample (75.86 mbsf).

Calculating the average relative diatom abundance across all samples revealed seven taxa that were observed at abundances > 5%: *Chaetoceros* resting spore type 1 (24.76%), *Rouxia naviculoides* (7.98%), *Chaetoceros* cf. *lorenzianus* (6.98%), *Rouxia antarctica* (6.58%), *Fragilariopsis barronii* (5.9%), *Thalassiosira inura* (5.22%) and *Denticulopsis simonsenii* (5.07%). The total abundance of these taxa is shown in Fig. 2D. While all these highly abundant taxa were present during both abundance peaks, *F. barronii* dominates the sharp diatom abundance peak at ~79.66 mbsf whereas *Chaetoceros* resting spores (type 1) characterise the second peak at ~76.86 mbsf. Abundances of all taxa identified in this study can be found in Table 1, and a photographic guide of all diatoms is provided in Supplementary Material B (Plates 1–17).

3.2. Environmental indicator species

A total of 18 diatom and silicoflagellate species identified in our samples were also recognised in Winter et al. (2010), and were assigned the same environmental preferences as in this latter study, specifically, for cold/sea-ice conditions: *Actinocyclus karstenii*, *Thalassiosira striata*, *Fragilariopsis curta*, *Rouxia antarctica*, *R. diploneides*, *R.* cf. *isopolica*, *R. naviculoides*; neritic/stratified: *Chaetoceros* resting spore types 1, 2, 9, *Thalassionema nitzschioides*; for warm conditions: *Shionodiscus oestrupii*, for mixed conditions: *Thalassiosira complicata*, *T. inura*, *Fragilariopsis praeinterfragidaria*; and for heavy/wind-mixed conditions: *Eucampia antarctica*, *Stephanopyxis turris*, *Stephanocha speculum* (Table 1).

Across most of the investigated period, the relative abundance of species belonging to the neritic/stratified category was most pronounced (22–77%), however, the cold/sea-ice group shows a higher relative abundance (~50%) at 80.16–79.46 and 77.56–77.36 mbsf (Fig. 2E). Relative abundances of taxa belonging to the cold/sea-ice and neritic/stratified categories were strongly negatively correlated (Pearson correlation coefficient $r = -0.84$), with higher (50%) and lower (30–40%) variation in the older and younger sediments (below and above ~77.56 mbsf, respectively; Fig. 2E). The cold/sea-ice and heavy/wind-mixed categories were positively ($r = 0.62$), and the neritic/stratified and heavy/wind-mixed categories negatively ($r = -0.66$) correlated while all other combinations were very weakly positively or negatively correlated (all r's between −0.17–0.16; Supplementary Material C).

Correlation analysis between all taxa and the ln-transformed Ba/Al data suggested the following species to be strongly positively correlated

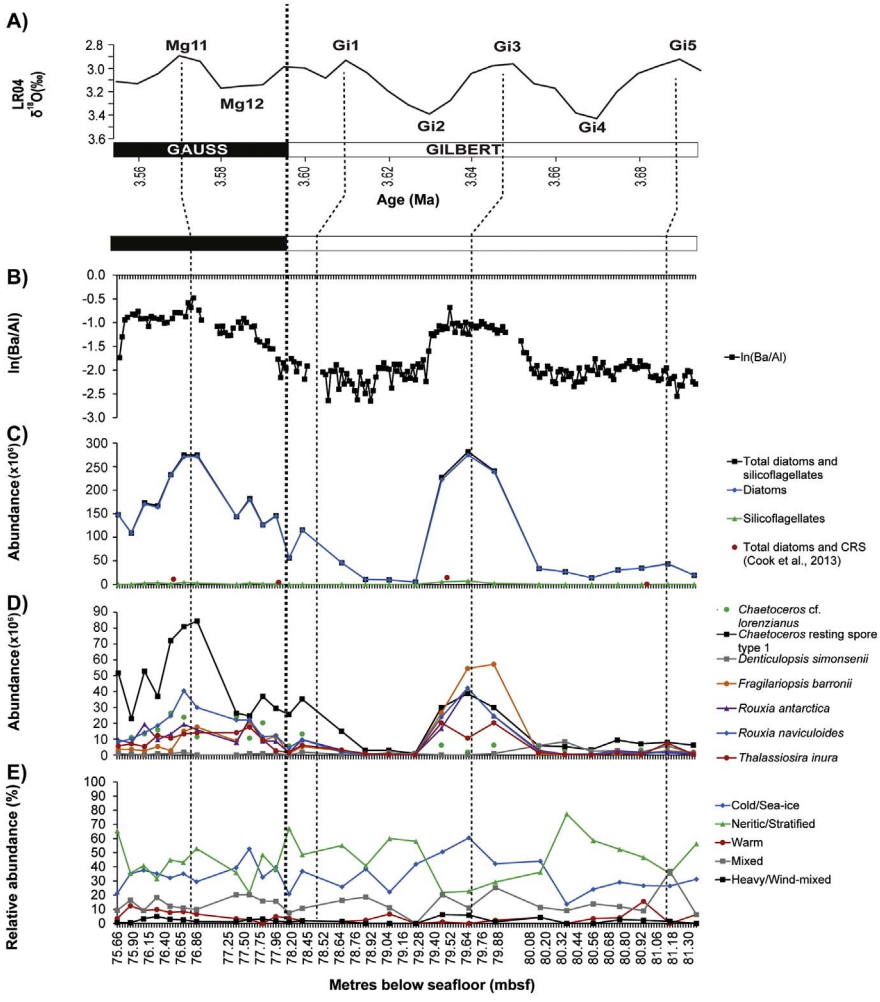

Fig. 2. Age model, diatom and silicoflagellate abundance and assemblage structure. A) Age model showing glacial (Gi4, Gi2, Mg12) and interglacial (Gi5, Gi3, Gi1, Mg11) cycles and the Gauss/Gilbert Boundary (3.6 Ma) based on LR04 oxygen isotope data. B) ln(Ba:Al) palaeo-productivity proxy record based on Cook et al. (2013). C) Total diatom (valves/g dry sediment) and silicoflagellates (skeletons/g dry sediment) abundance. The panel also includes the four diatom abundances from Cook et al. (2013) (red dots; CRS = *Chaetoceros* resting spores). D) Abundance of diatoms occurring on average > 5% across all samples (valves/g dry sediment). E) Relative abundance of taxa assigned to five environmental categories based on Winter et al. (2010) (for individual species and their abundance see Table 1).(For interpretation of the references to colour in this figure legend, the reader is referred to the web version of this article.)

with the palaeo-productivity proxy ln(Ba/Al): *Fragilariopsis weaveri* ($r = 0.86$), *Rouxia naviculoides* ($r = 0.82$), *Chaetoceros* resting spore type 1 ($r = 0.79$), *Rouxia diploneides*, *Shionodiscus oestrupii*, *Thalassiosira inura* (each $r = 0.77$, respectively), *Chaetoceros* cf. *lorenzianus* (0.71), *Rouxia antarctica* (0.69), *Fragilariopsis praeinterfragidaria* (0.68), and *Thalassionema nitzschioides* (0.62). *Denticulopsis simonsenii* showed the strongest negative correlation with ln(Ba/Al) ($r = -0.43$). For correlation coefficients between each taxon and ln(Ba/Al) see Supplementary Material D.

3.3. Age model

The age model by Cook et al. (2013) and Patterson et al. (2014) was refined based on our new results on diatom and silicoflagellate abundance and dominance of environmental indicator species as described in Section 3.2, matching interglacial periods with high diatom abundance and increased ln(Ba/Al) values, and glacial periods with low diatom abundance and low ln(Ba/Al) values (Fig. 2A, B, C). To refine our age model, we assumed a direct relationship between maximum warmth and phytoplankton abundance while acknowledging that an offset (e.g., maximum abundances preceding maximum warmth) may have occurred and cannot be excluded. We use the Marine Isotope Stages labelling convention defined by Lisiecki and Raymo (2005), with the naming being related to the magnetic reversal during which a stage occurs. Using this approach, the abundance peak in the upper/younger sediments (76.86 mbsf) was defined to be within Marine Isotope Stage Mg11 (3.57 Ma; interglacial) (Fig. 2A, C, D), and this is well constrained by the location of Gauss/Gilbert boundary (3.6 Ma) at 77.56 mbsf. We assigned the abundance peak in the older sediments (79.66 mbsf) to fall within Marine Isotope Stage Gi3 (3.65 Ma; interglacial; Fig. 2A, C, D). This is one Marine Isotope Stage younger than what Patterson et al. (2014) suggested for this interval (Gi5). The latter authors were careful to note that their one-to-one ties to the LR04 stack were not a unique solution. Indeed, correlation to the LR04 stack is subject to its own uncertainties due to potential out-of-phase relationships between southern and northern hemisphere orbital parameters, and thus a component of Antarctic climate and ice sheet variability could be hidden in this globally-integrated proxy of climate (Raymo et al., 2006). However, as we observe no intervening diatom assemblages consistent with interglacial conditions, we have tentatively assigned the interval to Gi3. We note that Gi3 and Gi5 are similar amplitude glacial cycles and thus this uncertainty has limited implications for our interpretation because the Gauss/Gilbert boundary at ~3.6 Ma separates high amplitude glacial-interglacial cycles (Marine Isotope Stages Gi5-Gi1) below from lower amplitude cycles above (Marine Isotope Stages Gi1-Mg11) (Fig. 2A). The reduction in the variation between cold/sea-ice and neritic/stratified species from 50% to 30–40% at ~77.56 mbsf coincides with this identification of the Gauss/Gilbert boundary (Fig. 2A, E). The high relative abundance of taxa belonging to the cold/sea-ice category especially around 79.66 mbsf is not contradictory to an interglacial period, as discussed below.

4. Discussion

4.1. Diatom and silicoflagellate assemblages between 81.36 and 75.66 mbsf (~3.69 and 3.56 Ma)

Microfossil counts revealed variable abundance of diatoms and the silicoflagellate *Stephanocha speculum* between 3.69 and 3.56 Ma. Two abundance peaks were identified during this time period (corresponding to depths between ~79.66 and ~76.86 mbsf), clearly refining the published productivity reconstruction by Cook et al. (2013). The latter study included four diatom valve counts and a nearly continuous Ba/Al record between 81.36 and 75.66 mbsf from Site U1361. Elevated diatom abundance (despite being lower than in our study, possibly due to methodological differences) and Ba/Al ratios in Cook et al. (2013) coincide with the here identified diatom abundance peaks, demonstrating consistency between the two studies and high productivity intervals during the two identified peak periods.

While low abundance intervals may reflect relatively low productivity at Site U1361A, the low abundance intervals directly preceding and following the abundance peak at 79.66 mbsf may be representative of an overbank turbidite deposit. The presence of such turbidite deposits has been associated with glacial conditions in this particular setting (Patterson et al., 2014), which, in our case appears to lead and trail the high productivity interval centred around ~79.66 mbsf.

This investigation has identified that while the diatom abundance peaks have similar valve concentrations and are composed of the same species, the relative abundance of these species differs greatly. This implies different environmental conditions were responsible for the increase in specific diatoms over others during abundance peak times, leading to the dominance of diatoms with differing ecological significance (i.e., phytoplankton composition during the two interglacial periods, 3.61–3.57 Ma and ~3.66–3.64 Ma, was not the same).

4.1.1. Microfossil assemblage during abundance peak at ~79.66 mbsf (~3.65 Ma)

During the first abundance peak, the pennate diatom *Fragilariopsis barronii* dominated the assemblage. *Fragilariopsis barronii* was not assigned to an environmental category as it was not listed in Winter et al. (2010) and because of its reported association with both sea-ice environments and stratification (making it difficult to assign it to either the cold/sea-ice or neritic/stratified category). For example, *F. barronii* has been identified in Pliocene sediments from the Sørsdal Formation, Vestfold Hills and the Prydz Bay ODP Site 1165 (East Antarctica; Fig. 1) where SSTs were estimated to have been warmer than today (Harwood et al., 2000; Whitehead and Bohaty, 2003; Escutia et al., 2009). In the same regions, *Fragilariopsis barronii* has also been reported to occur in meltwater/stratified open marine conditions in close proximity to sea-ice (Ross Sea and Sørsdal Formation; Bohaty et al., 1998; Harwood et al., 2000, respectively). The high abundance of *F. barronii* during the first abundance peak is, therefore, consistent with increased productivity intervals during interglacial conditions between ~79.46 and 80.16 mbsf identified by Cook et al. (2013). According to the latter study, interglacial conditions at this time were characterised by a marine ice sheet margin that had retreated significantly inland into the Wilkes Land subglacial basins, relative to the present day. Winter et al. (2010) found very low abundances of *F. barronii* in the AND-1B core, indicating that U1361A was more heavily influenced by seasonal sea-ice melt and/or surface water stratification/higher SSTs than the Ross Sea during this interglacial.

Both *Rouxia naviculoides* and *R. antarctica* also displayed high abundances during this distinct first abundance peak. The co-occurrence of these two species with *F. barronii* has been reported from Antarctic Pliocene sediments previously (Whitehead and McMinn, 2002). *Rouxia naviculoides* and *R. antarctica* have been described as cold water and sea-ice associated species that have (controversially) been found to augment in number when estimates of surface-water temperatures are considered to have increased to ~5 °C (Whitehead and McMinn, 2002; Escutia et al., 2009; Winter et al., 2012b). Elsewhere, *Rouxia* spp. were commonly encountered near the sea-ice in the Ross Sea in relatively low salinity waters (Bohaty et al., 1998; Sjunneskog and Winter, 2012) and were categorised as cold/sea-ice species by Winter et al. (2010). *Chaetoceros* resting spore type 1 and *Thalassiosira inura* also figured as highly abundant species during this first abundance peak, and strongly correlated with ln(Ba/Al). Based on Winter et al. (2010), we assigned *Chaetoceros* resting spores and *T. inura* to the neritic/stratified and mixed category, respectively, in this study. The only silicoflagellate encountered (in very low abundances) was *Stephanocha speculum,* which generally occurs in cold surface waters (< 6 °C; based on modern observations; Rigual-Hernández et al.,

2016). Winter et al. (2010) classify silicoflagellates as belonging to the heavy/wind-mixed category. Considering the high abundance of *Rouxia* spp. belonging to the cold/sea-ice category concurrent with *F. barronii*, *Chaetoceros* resting spores, *T. inura*, and low abundances of *S. speculum*, we define the period between 80.16 and 79.26 mbsf (within Marine Isotope Stage Gi3) as an interglacial period characterised by elevated SSTs, marginal glacial or sea-ice meltwater leading to stratification at Site U1361A. It is possible, that during this time, seasonal sea-ice cover existed at our study site (to a heavier extent than in the Ross Sea, as described above).

4.1.2. Microfossil assemblage during abundance peak at 78.86–76.66 msbf (~3.61–3.57 Ma)

During the younger abundance peak, the dominant species was *Chaetoceros* resting spores (type 1). Resting spores of this genus were classified as neritic/stratified in this study as previously attributed by Winter et al. (2010). In the Southern Ocean, highest abundances of *Chaetoceros* resting spores have been shown to occur near the West Antarctic Peninsula, where the seasonal melting of sea-ice induces stratification, resulting in reduced nutrient supply (Crosta et al., 1997; Leventer et al., 2002). In East Antarctica, *Chaetoceros* resting spores were associated with stratified open water (Whitehead et al., 2001). Previous studies by Whitehead and Bohaty (2003), Escutia et al. (2009); Winter et al. (2010), and Cook et al. (2013) have all reported a retreated sea-ice extent resulting from elevated SSTs during the time just following the Gauss/Gilbert boundary. Using Nd and Sr isotope data, Cook et al. (2013) infer an ice sheet retreat that deviated greatly from the Holocene (higher Nd and lower $^{87}Sr/^{86}Sr$). Interpolations of SST to the Wilkes Land margin used by Cook et al. (2013, and references therein), assumes a warm period characterised by > 4 °C above modern SSTs between 77.96 and 77.56 mbsf, and two warm intervals > 2.5 °C above modern SSTs around ~76.86 and 76.46 mbsf at Site U1361. These periods were reported to have been characterised by ice-free open water conditions and increased productivity at this site (Cook et al., 2013). It is speculated here that the repeated short, warm intervals between 77.96 and 76.46 mbsf reported by Cook et al. (2013) may have stimulated the gradual increase of phytoplankton (especially *Chaetoceros* vegetative and resting forms) productivity regionally.

Other species that belonged to the most abundant species during the abundance peak in the younger sediment (although abundant to a much lesser degree than *Chaetoceros* resting spore type 1), were *R. naviculoides*, *R. antarctica, Chaetoceros* cf. *lorenzianus*, *F. barronii* and *T. inura*. All five species were moderately to strongly correlated to the palaeoproxy ln(Ba/Al) in this study, indicating interglacial conditions at the time of the younger abundance peak (~3.57 Ma; Mg11). Based on Winter et al. (2010), *Rouxia* spp. indicate cold/sea-ice conditions (see Section 4.1.1), while *T. inura* was classified as preferring mixed water conditions. *Thalassiosira inura* has also been associated with warm SSTs previously (Fig. 6 in Harwood et al., 2000). Konfirst et al. (2011) showed that *Shionodiscus tetraoestrupii* (warm-water indicator) increased in abundance relative to *Rouxia* spp. (cold-water indicator) between Mg12 and Mg11 in the AND-1B core. More generally, a shift from *Shionodiscus tetraoestrupii* to *Rouxia* spp., which was interpreted by Konfirst et al. (2011) to occur over several glacial-interglacial variations from Gi2 to Mg11 (subunit 3) with an anti-correlated abundance of these two taxa. However, their age model differed from that of McKay et al. (2012) who assigned this shift to a warmer, less sea-ice tolerant, diatom assemblage to occur entirely within the normal polarity zone of the Gauss and was therefore younger than 3.58 Ma (e.g., Mg12 to Mg11).

The high abundance of *Chaetoceros* resting and vegetative forms alongside species indicative of meltwater, stratification and warm conditions between 78.86 and 76.66 mbsf in this study suggests that seasonally prolonged open marine conditions were more prevalent at Site U1361A around 76.86 mbsf (~3.58 Ma) compared to 79.66 mbsf (~3.64 Ma). This scenario agrees with the finding from ANDRILL and Prydz Bay suggesting SSTs between 2.7 and 4 °C above modern at 3.58 Ma (Gauss/Gilbert boundary) were contemporaneous with the reduction of the Antarctic Peninsula Ice Sheet and the EAIS (Escutia et al., 2009; McKay et al., 2012). Recent model simulations suggest warm Pliocene conditions may have resulted in significant surface ice sheet melt processes that contributed to rapid ice sheet collapse event into the Wilkes subglacial basin (DeConto and Pollard, 2016), and may have contributed in part to the increased stratification in this interval. However, meltwater associated with increased seasonal sea-ice extent may have played a large role, too. Although increased sea-ice is counterintuitive in a warmer world, a deglaciated Wilkes subglacial basin provides a larger continental shelf area (and at higher latitudes) for winter sea-ice to form, and, therefore, enhanced spring melting of this sea-ice in the warmer Pliocene climates may have contributed to enhanced stratification. An additional feedback is that of increased katabatic winds that were modelled to have been diverted into this region during Pliocene deglaciations (Scherer et al., 2016; Fig. 1). These winds may have enhanced polynya-driven sea-ice production that was transported offshore towards the open ocean. If this was the case, then the melting of the sea-ice while progressing northwards may have further resulted in increased stratification at our study site.

4.1.3. Diatoms and silicoflagellates indicating cold, low productivity intervals

Denticulopsis simonsenii was determined as the eighth most abundant diatom in our study. However, maximum abundance of *D. simonsenii* did not fall into either of the two abundance peaks. Moreover, highest abundance of *D. simonsenii* (8×10^6 valves/g dry sediment) was encountered at ~80.36 mbsf, a period identified as a cold and low productivity interval by Cook et al. (2013) and this study. *Denticulopsis simonsenii* has been judged as a cosmopolitan diatom, with origins from the mid- to high-latitudes, but more often encountered across all latitudes since a major cooling in the middle Miocene (Barron, 1986). The species' higher abundance and longer stratigraphic range in mid- to high-latitudes might indicate its preference for permanently cold regions (< 2.5 °C warmer than modern SST). Considering the relatively high abundance of *D. simonsenii,* which was strongly negatively associated with the palaeo-productivity proxy ln(Ba/Al), and the concurrent relatively high abundance of the neritic/stratified category at 80.36 mbsf, we speculate that intermediate conditions prevailed at this time (~3.67–3.66 Ma), potentially marking the transition from glacial to interglacial and matching the onset of Gi3.

4.1.4. Age model constraints using diatom and silicoflagellate data

Investigating diatom and silicoflagellate abundance and environmental indicator species allowed us to further constrain the age model used by Cook et al. (2013) and Patterson et al. (2014). Our data confirm peaks in diatom (and silicoflagellate) abundance during the interglacial Gi3 and across the Gauss/Gilbert boundary, temporally consistent with high productivity intervals previously identified by Cook et al. (2013). While diatom and silicoflagellate abundance is similar during both interglacials we identified a large variation in the assemblages, indicating differences not only between glacial and interglacial but also between different interglacial periods. In particular, our suggestion of warmer and more stratified water masses around 3.58 Ma correspond to an increased deglaciation of the EAIS Wilkes Land subglacial basin, as inferred by trace element provenance data of Cook et al. (2013), relative to the earlier high productivity interval around ~3.65 Ma, which has been shown to have an ice sheet erosional provenance signature similar to the Holocene.

5. Conclusion

Fossilised diatom assemblage was investigated from the Exp. 318 Site U1361A at the Antarctic Wilkes Land margin in Pliocene sediments from 81.36–75.66 mbsf (~3.69–3.56 Ma). Two abundance peaks were

identified, one short and abrupt around 79.66 mbsf (~3.65 Ma, Gi3), and one gradual increase peaking at 76.86 mbsf (~3.58 Ma, following the Gauss/Gilbert boundary). While diatom assemblages were similar, relative abundances showed high variability throughout four glacial/interglacial cycles. Eighteen taxa could be classified as environmental indicator species based on previous investigations. It is suggested (consistent with Cook et al., 2013) that sea-ice was greatly reduced at Site U1361A during the investigated time frame, with seasonal sea-ice cover and associated meltwater influence during Gi3, and prolonged ice-free open water conditions across the Gauss/Gilbert boundary. The results of Cook et al. (2013) through this important transitional stage of the Pliocene were refined, both in terms of diatom/silicoflagellate assemblage resolution and age determination of the investigated sediments.

Supplementary data to this article can be found online at https://doi.org/10.1016/j.marmicro.2017.10.008.

Acknowledgements

We thank the International Ocean Discovery Program (IODP), which provided the samples, and the Australia-New Zealand IODP Consortium (ANZIC), which provided Special Analytical Funding (LE140100047) for this particular study. Additional funding was provided by the Spanish Ministry of Science and Innovation Grant CTM2014-60451-C2-1-P co-financed by the European Regional Development Fund (FEDER). This work was also supported by the Japan Society for Promotion of Science (JSPS) KAKENHI Grant Number 25550015 and the Royal Society of New Zealand Rutherford Discovery Fellowship (RDF-13-VUW-003). Many thanks go to Andrés Rigual-Hernández for his help with logistics and in the laboratory, to David Harwood for his assistance with diatom identifications, to Amy Leventer and Xavier Crosta for constructive discussions and to the anonymous reviewers for valuable feedback.

References

Armand, L.K., Leventer, A., 2010. Palaeo sea-ice distribution and reconstruction derived from the geological records. In: Thomas, D.N., Dieckmann, G.S. (Eds.), Sea Ice. John Wiley & Sons, Ltd., Chichester, West Sussex, UK, pp. 469–530.

Armand, L., Ferry, A., Leventer, A., 2017. Advances in palaeo sea-ice estimation. In: Thomas, D.N. (Ed.), Sea Ice. Wiley-Blackwell, pp. 600–629.

Bamber, J.L., Aspinall, W.P., 2013. An expert judgement assessment of future sea level rise from the ice sheets. Nat. Clim. Chang. 3, 424–427.

Barron, J.A., 1986. Paleoceanographic and tectonic controls on deposition of the Monterey Formation and related siliceous rocks in California. Palaeogeogr. Palaeoclimatol. Palaeoecol. 53, 27–45.

Bart, P.J., Iwai, M., 2012. The overdeepening hypothesis: how erosional modification of the marine-scape during the early Pliocene altered glacial dynamics on the Antarctic Peninsula's Pacific margin. Palaeogeogr. Palaeoclimatol. Palaeoecol. 355, 42–51.

Bohaty, S.M., Scherer, R.P., Harwood, D.M., 1998. Quaternary diatom biostratigraphy and paleoenvironments of the CRP-11 drillcore, Ross Sea, Antarctica. Terra Antarct. 5, 431–453.

Cook, C.P., van de Flierdt, T., Williams, T., Hemming, S.R., Iwai, M., Kobayashi, M., Jimenez-Espejo, F.J., Escutia, C., González, J.J., Khim, B.K., McKay, R.M., Passchier, S., Bohaty, S.M., Riesselman, C.R., Tauxe, L., Sugisaki, S., Galindo, A.L., Patterson, M.O., Sangiorgi, F., Pierce, E.L., Brinkhuis, H., Klaus, A., Fehr, A., Bendle, J.A.P., Bijl, P.K., Carr, S.A., Dunbar, R.B., Flores, J.A., Hayden, T.G., Katsuki, K., Kong, G.S., Nakai, M., Olney, M.P., Pekar, S.F., Pross, J., Röhl, U., Sakai, T., Shrivastava, P.K., Stickley, C.E., Tuo, S., Welsh, K., Yamane, M., 2013. Dynamic behaviour of the East Antarctic ice sheet during Pliocene warmth. Nat. Geosci. 6, 765–769.

Crosta, X., Pichon, J.J., Labracherie, M., 1997. Distribution of *Chaetoceros* resting spores in modern peri-Antarctic sediments. Mar. Micropaleontol. 29, 283–299.

DeConto, R.M., Pollard, D., 2016. Contribution of Antarctica to past and future sea-level rise. Nature 531, 591–597.

Dowsett, H.J., Haywood, A.M., Valdes, P.J., Robinson, M.M., Lunt, D.J., Hill, D.J., Stoll, D.K., Foley, K.M., 2011. Sea surface temperatures of the mid-Piacenzian warm period: a comparison of PRISM3 and HadCM3. Palaeogeogr. Palaeoclimatol. Palaeoecol. 309, 83–91.

Dutton, A., Carlson, A.E., Long, A.J., Milne, G.A., Clark, P.U., DeConto, R., Horton, B.P., Rahmstorf, S., Raymo, M.E., 2015. Sea-level rise due to polar ice-sheet mass loss during past warm periods. Science 349, 153–162.

Escutia, C., Bárcena, M.A., Lucchi, R.G., Romero, O., Ballegeer, A.M., Gonzalez, J.J., Harwood, D.M., 2009. Circum-Antarctic warming events between 4 and 3.5 Ma recorded in marine sediments from the Prydz Bay (ODP Leg 188) and the Antarctic Peninsula (ODP Leg 178) margins. Glob. Planet. Chang. 69, 170–184.

Escutia, C., Brinkhuis, H., Klaus, A., the Exp. 318 Scientists, 2011. Expedition 318 summary. In: Proceedings of the Integrated Ocean Drilling Program. vol. 318. pp. 1–59.

Fetterer, F., Knowles, K., Meier, W., Savoie, M., Windnagel, A.K., 2016. Sea Ice Index, Version 2. [median sea-ice extent]. NSIDC: National Snow and Ice Data Center, Boulder, Colorado USA updated daily. https://doi.org/10.7265/N5736NV7 (Date Accessed: Nov. 2015).

Golledge, N.R., Kowalewski, D.E., Naish, T.R., Levy, R.H., Fogwill, C.J., Gasson, E.G.W., 2015. The multi-millennial Antarctic commitment to future sea-level rise. Nature 526, 421–425.

Golledge, N.R., Levy, R.H., Naish, T.R., McKay, R.M., Edward, G.W., Kowalewski, D.E., Fogwill, C.J., 2016. Antarctic contribution to global sea level in a high CO_2 world. Geophys. Res. Abstr. 18, 2016 (EGU2016-1407, EGU General Assembly).

Golledge, N.R., Levy, R.H., McKay, R.M., Naish, T.R., 2017. East Antarctic ice sheet most vulnerable to Weddell Sea warming. Geophys. Res. Lett. 44, 2343–2351.

Grützner, J., Hillenbrand, C.D., Rebesco, M., 2005. Terrigenous flux and biogenic silica deposition at the Antarctic continental rise during the late Miocene to early Pliocene: implications for ice sheet stability and sea ice coverage. Glob. Planet. Chang. 45, 131–149.

Harwood, D.M., McMinn, A., Quilty, P.G., 2000. Diatom biostratigraphy and age of the Pliocene Sørsdal Formation, Vestfold Hills, East Antarctica. Antarct. Sci. 12, 443–462.

Haywood, A.M., Hill, D.J., Dolan, A.M., Bragg, F., Chan, W., Chandler, M.A., 2013. Large-scale features of Pliocene climate: results from the Pliocene Model Intercomparison Project. Clim. Past 9, 191–209.

Hobbs, W.R., Massom, R., Reid, P.A., Meier, W., Massom, R., Stammerjohn, S., Reid, P., Williams, G., Meier, W., 2016. A review of recent changes in Southern Ocean sea ice, their drivers and forcings. Glob. Planet. Chang. 143, 228–250.

IPCC, 2013. Summary for policymakers. In: Stocker, T.F., Qin, D., Plattner, G.-K., Tignor, M., Allen, S.K., Boschung, J., Nauels, A., Xia, Y., Bex, V., Midgley, P.M. (Eds.), Climate Change 2013: The Physical Science Basis. Contribution of Working Group I to the Fifth Assessment Report of the Intergovernmental Panel on Climate Change. Cambridge University Press, Cambridge, United Kingdom and New York, NY, USA.

Jones, J., Gille, S., Goosse, H., Abram, N., Canziani, P., Charman, D., Clem, K., Crosta, X., De Lavergne, C., Eisenman, I., England, M., Fogt, R., Frankcombe, L.M., Marshall, G., Masson-Delmotte, V., Morrison, A., Orsi, A., Raphael, M., Renwick, J., Schneider, D., Simpkins, G., Steig, E., Stenni, B., Swingedouw, D., Vance, T., 2016. Assessing recent trends in high-latitude Southern Hemisphere surface climate. Nat. Clim. Chang. 6 (10). http://dx.doi.org/10.7589/2012-06-150.

Jordan, R.W., McCartney, K., 2015. *Stephanocha nom. nov.*, a replacement name for the illegitimate silicoflagellate genus *Distephanus* (Dictyochophyceae). Phytotaxa 201, 177–187.

Koizumi, I., Tanimura, Y., 1985. Neogene diatom biostratigraphy of the middle latitude western North Pacific, Deep Sea Drilling Project Leg 86. In: Initial Reports DSDP Leg. 86. pp. 269–300.

Konfirst, M.A., Kuhn, G., Monien, D., Scherer, R.P., 2011. Correlation of Early Pliocene diatomite to low amplitude Milankovitch cycles in the ANDRILL AND-1B drill core. Mar. Micropaleontol. 80 (3), 114–124.

Leventer, A., Domack, E., Barkoukis, A., McAndrews, B., Murray, J., 2002. Laminations from the Palmer Deep: a diatom-based interpretation. Paleoceanography 17 (3). http://dx.doi.org/10.1029/2001pa000624.

Lisiecki, L.E., Raymo, M.E., 2005. A Pliocene-Pleistocene stack of 57 globally distributed benthic $\delta^{18}O$ records. Paleoceanography 20. http://dx.doi.org/10.1029/2004PA001071.

McKay, R., Naish, T., Carter, L., Riesselman, C., Dunbar, R., Sjunneskog, C., Winter, D., Sangiorgi, F., Warren, C., Pagani, M., Schouten, S., Willmott, V., Levy, R., DeConto, R., Powell, R.D., 2012. Antarctic and Southern Ocean influences on Late Pliocene global cooling. Proc. Natl. Acad. Sci. U. S. A. 109, 6423–6428.

Naish, T.R., Powell, R.D., Levy, R., Wilson, G.S., Scherer, R.P., Talarico, F., Krissek, L.A., Niessen, F., Pompilio, M., Wilson, T., Carter, L., DeConto, R.M., Huybers, P., McKay, R.M., Pollard, D., Ross, J., Winter, D., Barrett, P., Browne, G., Cody, R., Cowan, E.A., Crampton, J., Dunbar, G., Dunbar, N., Florindo, F., Gebhardt, C., Graham, I., Hannah, M., Hansaraj, D., Harwood, D.M., Helling, D., Henrys, S., Hinnov, L.A., Kuhn, G., Kyle, P., Läufer, A., Maffioli, P., Magens, D., Mandernack, K., McIntosh, W., Millan, C., Morin, R., Ohneiser, C., Paulsen, T., Persico, D., Raine, I., Reed, J., Riesselman, C.R., Sagnotti, L., Schmitt, D., Sjunneskog, C., Strong, P., Taviani, M., Vogel, S., Wilch, T., Williams, T., 2009. Obliquity-paced Pliocene West Antarctic ice sheet oscillations. Nature 458, 322–328.

Pagani, M., Liu, Z., Lariviere, J., Ravelo, A.C., 2009. High Earth-system climate sensitivity determined from Pliocene carbon dioxide concentrations. Nat. Geosci. 3, 27–30.

Patterson, M.O., McKay, R., Naish, T., Escutia, C., Jimenez-Espejo, F.J., Raymo, M.E., Meyers, S.R., Tauxe, L., Brinkhuis, H., Klaus, A., Fehr, A., Bendle, J.A.P., Bijl, P.K., Bohaty, S.M., Carr, S.A., Dunbar, R.B., Flores, J.A., Gonzalez, J.J., Hayden, T.G., Iwai, M., Katsuki, K., Kong, G.S., Nakai, M., Olney, M.P., Passchier, S., Pekar, S.F., Pross, J., Riesselman, C.R., Röhl, U., Sakai, T., Shrivastava, P.K., Stickley, C.E., Sugasaki, S., Tuo, S., van de Flierdt, T., Welsh, K., Williams, T., Yamane, M., 2014. Orbital forcing of the East Antarctic ice sheet during the Pliocene and Early Pleistocene. Nat. Geosci. 7, 841–847.

Pollard, D., DeConto, R.M., 2009. Modelling West Antarctic ice sheet growth and collapse through the past five million years. Nature 458, 329–332.

Pollard, D., DeConto, R.M., Alley, R.B., 2015. Potential Antarctic Ice Sheet retreat driven by hydrofracturing and ice cliff failure. Earth Planet. Sci. Lett. 412, 112–121.

Raymo, M.E., Lisiecki, L.E., Nisancioglu, K.H., 2006. Plio-Pleistocene ice volume, Antarctic climate, and the global $\delta^{18}O$ record. Science 313, 492–495.

Reinardy, B.T.I., Escutia, C., Iwai, M., Jimenez-Espejo, F.J., Cook, C., van de Flierdt, T., Brinkhuis, H., 2015. Repeated advance and retreat of the East Antarctic Ice Sheet on the continental shelf during the early Pliocene warm period. Palaeogeogr. Palaeoclimatol. Palaeoecol. 422, 65–84.

Rigual-Hernández, A.S., Trull, T.W., McCartney, K., Ballegeer, A.M., Lawler, K.A., Bray, S.G., Armand, L.K., 2016. Indices based on silicoflagellate assemblages offer potential for paleo-reconstructions of the main oceanographic zones of the Southern Ocean. Geo-Mar. Lett. 36, 271–280.

Ryan, W.B.F., Carbotte, S.M., Coplan, J.O., O'Hara, S., Melkonian, A., Arko, R., Weissel, R.A., Ferrini, V., Goodwillie, A., Nitsche, F., Bonczkowski, J., Zemsky, R., 2009. Global multi-resolution topography synthesis. Geochem. Geophys. Geosyst. 10. http://dx.doi.org/10.1029/2008GC002332.

Scherer, R.P., DeConto, R.M., Pollard, D., Aller, R.B., 2016. Windblown Pliocene diatoms and East Antarctic Ice Sheet retreat. Nat. Commun. 7, 1–9.

Schrader, H.J., Gersonde, R., 1978. Diatoms and silicoflagellates. In: Zachariasse, W.J., Riedel, W.R., Sanfilippo, A., Schmidt, R.R., Brolsma, M.J., Schrader, H.J., Gersonde, R., Drooger, M.M., Broekman, J.A. (Eds.), Micropalaeontological Counting Methods and Techniques - an Excercise on an Eight Metres Section of the Lower Pliocene of Capo Rossello, Sicily. Utrecht Micropal. Bull., vol. 17. pp. 129–176.

Scientific Committee on Antarctic Research, (no date), SCAR Antarctic Digital Database 6. 0. http://www.scar.org/add.

Seki, O., Foster, G.L., Schmidt, D.N., Mackensen, A., Kawamura, K., Pancost, R.D., 2010. Alkenone and boron-based Pliocene pCO_2 records. Earth Planet. Sci. Lett. 292, 201–211.

Sjunneskog, C., Winter, D., 2012. A diatom record of late Pliocene cooling from the Ross Sea continental shelf, AND-1B, Antarctica. Glob. Planet. Chang. 96–97, 87–96.

Vasskog, K., Langebroek, P.M., Andrews, J.T., Even, J., Nilsen, Ø., Nesje, A., 2015. The Greenland Ice Sheet during the last glacial cycle: current ice loss and contribution to sea-level rise from a palaeoclimatic perspective. Earth Sci. Rev. 150, 45–67.

Whitehead, J.M., Bohaty, S.M., 2003. Pliocene summer sea surface temperature reconstruction using silicoflagellates from Southern Ocean ODP Site 1165. Paleoceanography 18, 1–11.

Whitehead, J.M., McMinn, A., 2002. Kerguelen Plateau Quaternary late Pliocene palaeoenvironments: from diatom, silicoflagellate and sedimentological data. Palaeogeogr. Palaeoclimatol. Palaeoecol. 186, 335–368.

Whitehead, J.M., Quilty, P.G., Harwood, D.M., McMinn, A., 2001. Early Pliocene paleoenvironment of the Sørsdal Formation, Vestfold Hills, based on diatom data. Mar. Micropaleontol. 41, 125–152.

Williams, T., van de Flierdt, T., Hemming, S.R., Chung, E., Roy, M., Goldstein, S.L., 2010. Evidence for iceberg armadas from East Antarctica in the Southern Ocean during the late Miocene and early Pliocene. Earth Planet. Sci. Lett. 290, 351–361.

Winter, D., Sjunneskog, C., Harwood, D., 2010. Early to mid-Pliocene environmentally constrained diatom assemblages from the AND-1B drillcore, McMurdo Sound, Antarctica. Stratigraphy 7, 207–227.

Winter, D., Sjunneskog, C., Scherer, R., Maf, P., Harwood, D., 2012a. Diatom-based correlation of early to mid-Pliocene drillcores from the southwestern Ross Sea, Antarctica. Glob. Planet. Chang. 96–97, 131–142.

Winter, D., Sjunneskog, C., Scherer, R., Maffioli, P., Riesselman, C., Harwood, D., 2012b. Pliocene-Pleistocene diatom biostratigraphy of nearshore Antarctica from the AND-1B drillcore, McMurdo Sound. Glob. Planet. Chang. 96–97, 59–74.

Zachos, J.C., Dickens, G.R., Zeebe, R.E., 2008. An early Cenozoic perspective on greenhouse warming and carbon-cycle dynamics. Nature 451, 279–283.

Zielinski, U., 1993. Quantitative estimation of palaeoenvironmental parameters of the Antarctic Surface Water in the Late Quaternary using transfer functions with diatoms. Ber. Polarforsch. 126, 1–148.